Supporting Information

In Situ Synthesis of Ultrasmall MnO Nanoparticles Encapsulated by Nitrogen-doped Carbon Matrix for High-performance Lithium-ion Batteries

Shi Tao, [*a] Biao Li, [b] Jingyuan Zhang, [a] Peixin Cui, [c] Dajun Wu, [a] Wangsheng Chu, [d] Bin Qian, [*a] Li Song [*d]

[a] Department of Physics and Electronic Engineering, Jiangsu Laboratory of Advanced Functional Materials, Changshu Institute of Technology, Changshu 215500, China

[b] Department of Energy and Resources, College of Engineering，Peking University, 100871, China

[c] Key Laboratory of Soil Environment and Pollution Remediation Institute of Soil Science, Chinese Academy of Sciences, 210008, China

[d] National Synchrotron Radiation Laboratory, University of Science and Technology of China, 230029, China

Experimental section

Chemicals

All chemicals were purchased and used without further purification. Manganese nitrate tetrahydrate [$Mn(NO_3)\cdot 4H_2O$], N,N-Dimethylformamide (DMF) and triethylamine (TEA) were obtained from Sinopharm Chemical Reagent Shanghai Co.. Ethylenediaminetetraacetic acid (H_4EDTA) was purchased from Sigma-Aldrich

(USA).

Synthesis of MnO@NDC precursors

8 mmol $Mn(NO_3)\cdot 4H_2O$ were dissolved into 40 mL DMF forming a solution, then added to a DMF solution of H_4EDTA (4 mmol) with 1.5 mL triethylamine. A precipitate was filtered and washed with DMF. The obtained white powder were collected after vacuum drying at 60 ℃ for overnight. The highly dispersed [Mn_2(EDTA)] precursors were annealed from room temperature to 500-600 ℃ at a heating rate of 2 min^{-1} in N_2 atmosphere for 2 h. The Mn_2O_3 sample was synthesized by annealing the MnO@NDC at 500 ℃ for 2h in the air atmosphere.

Material Characterization

The X-ray powder diffraction (XRD) pattern was recorded by a Bruker D8 ADVANCE X-ray diffractometer with Cu K_α radiation (λ = 0.15418 nm) at a scanning rate of 4° min^{-1}. Field-emmision scanning electron microscopy (SEM) images were obtained on a ZEISS microscope with an accelerating voltage of 20 kV. Transmission electron microscopy (TEM) images and high-resolution TEM (HRTEM) images were obtained by a JEOL JEM-2000CX instrument. Nitrogen adsorption and desorption isotherm was characterized by a ASAP2020. The XPS experiments were carried out on a PHI-5400 electron spectrometer. The Raman spectrum was performed by a Raman spectrometer (Horiba Xplora). The thermogravimetric analysis (TGA) was conducted on a thermogravimetric analyzer (TGA, SDTA851). Mn K-edge XAFS spectra of samples were recorded at the BL14W1 beamline of Shanghai synchrotron radiation facility (SSRF). To get the desired electrodes, the coin cells

were charged/discharged to the desired cutoff voltages and dissembled. The disassembled electrodes were washed with dimethyl carbonate (DMC) in the Ar-filled glove box, after drying, the electrodes were sealed by a 3M selloptape.

Electrochemical Measurements

The working electrode was prepared by mixing the MnO@NDC powder, acetylene black, and polyvinylidene difluoride (PVDF) in a weight ratio of 70:20:10. The slurry was pasted to Cu foil for LIBs, and then dried at 100 °C overnight under vacuum. CR2032-type coin cells were assembled in an argon-filled glovebox. For LIBs half-cells, Li-metal foil use as counter electrode, and 1.0 M $LiPF_6$ dissolved in ethylene carbonate (EC)/dimethl carbonat (DMC)/diethyl carbonate (DEC) (1:1:1 by volume) use as electrolyte. The charge-discharge tests were carried out on LAND CT2001A systems. The cyclic voltammetry (CV) curves and electrochemical impedance spectroscopy (EIS) were tested on VSP electrochemical workstation (Bio-logic, France).

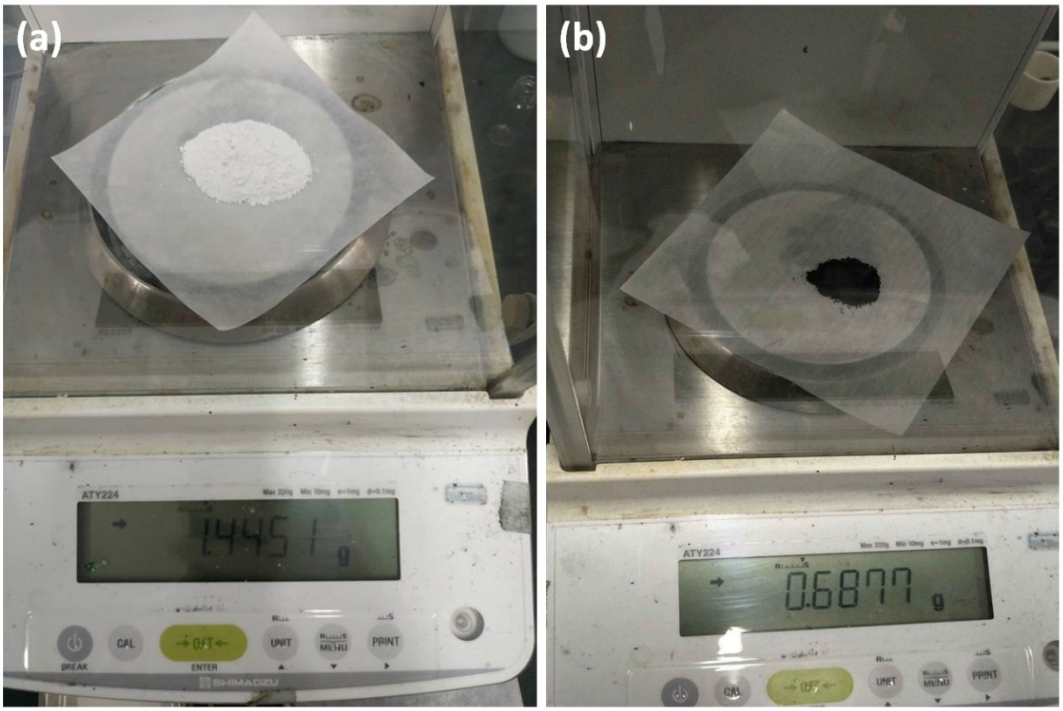

Figure S1. (a) Weight of the [Mn_2(EDTA)] precursors. (b)Weight of the MnO@NDC powder.

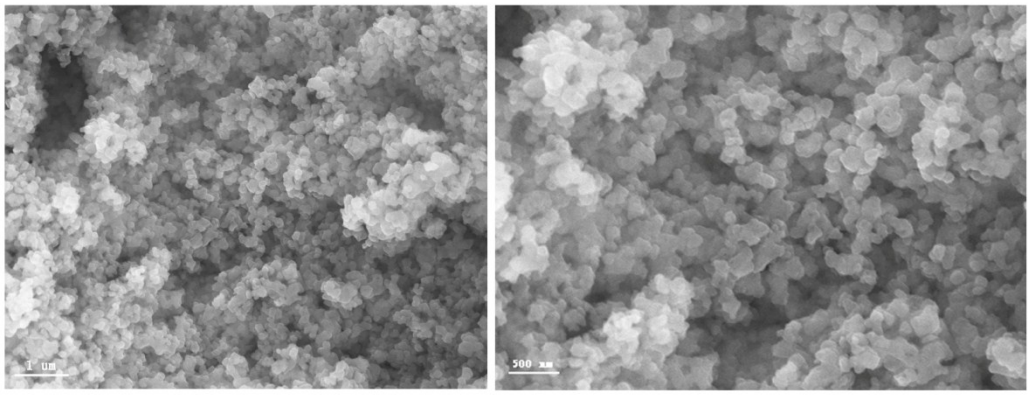

Figure S2. SEM images of the [Mn_2(EDTA)] precursors.at different magnification.

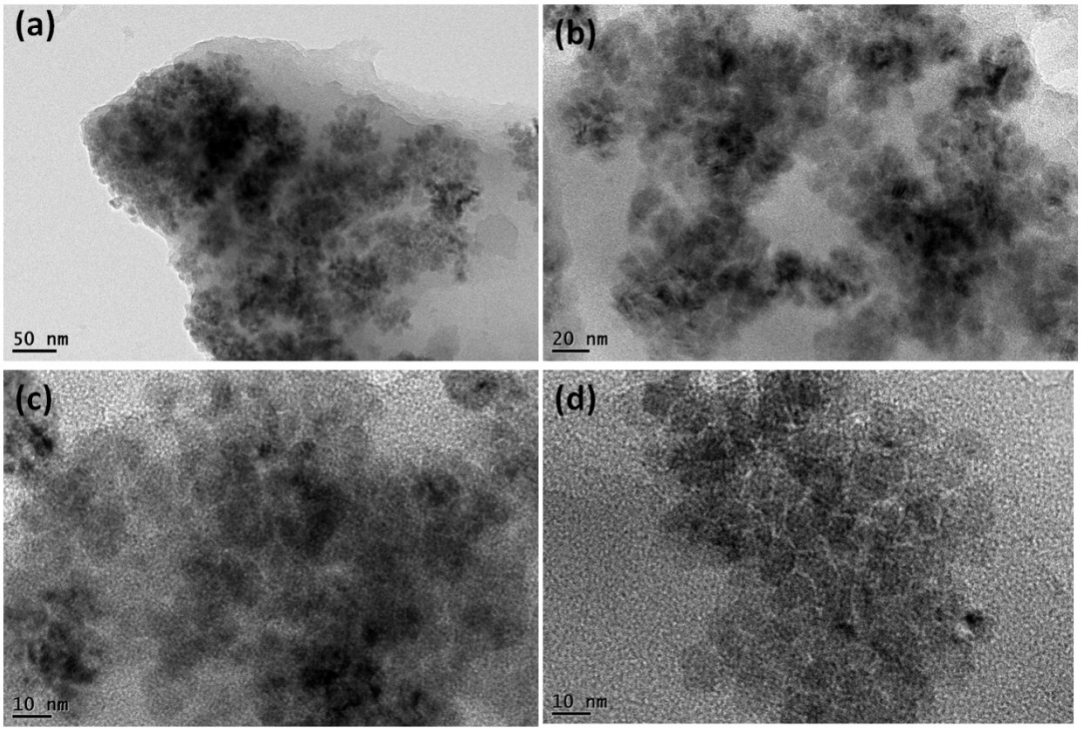

Figure S3. TEM images of MnO@NDC at different magnitude resolution.

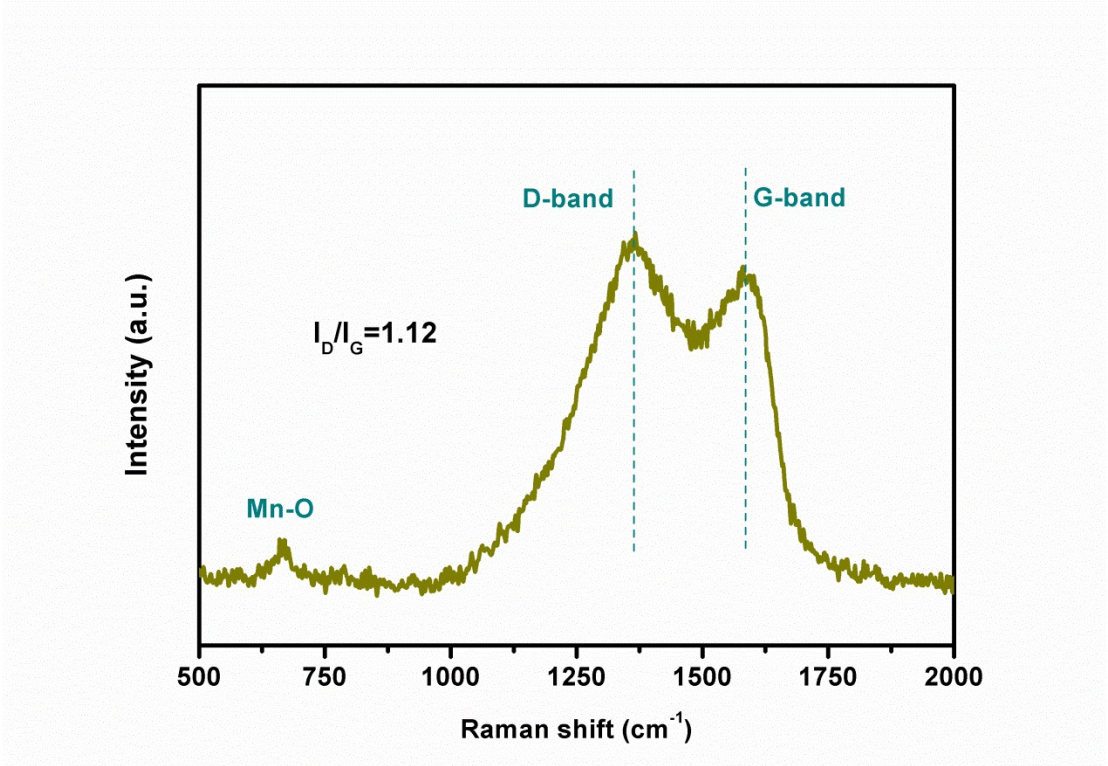

Figure S4. Raman spectra of the MnO@NDC.

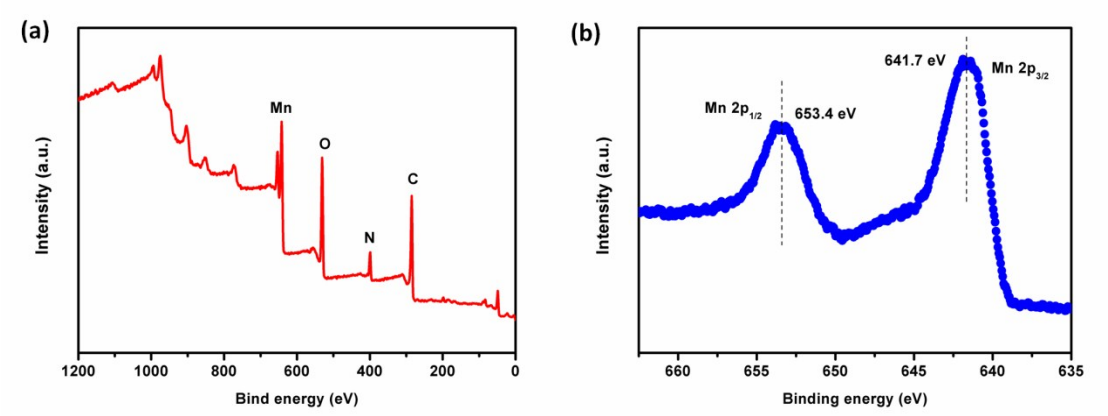

Figure S5. (a) XPS survey spectrum of MnO@NDC. (b) High-resolution XPS spectra of Mn 2p.

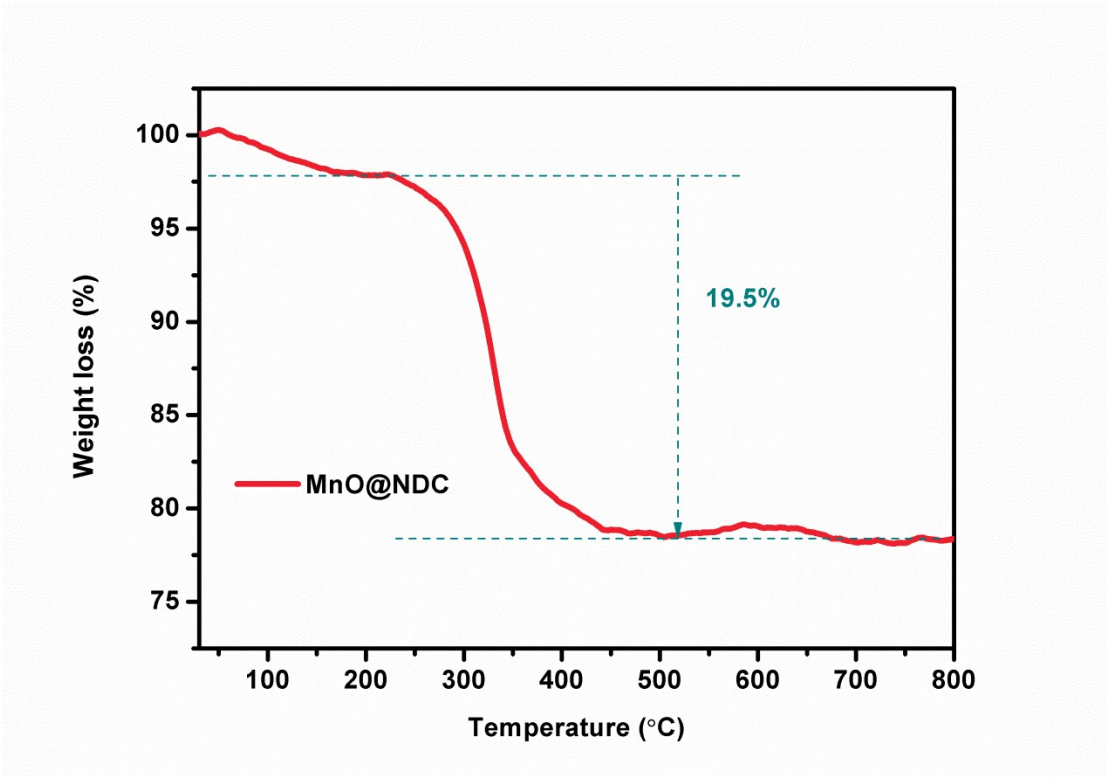

Figure S6. TGA curve of the MnO@NDC.

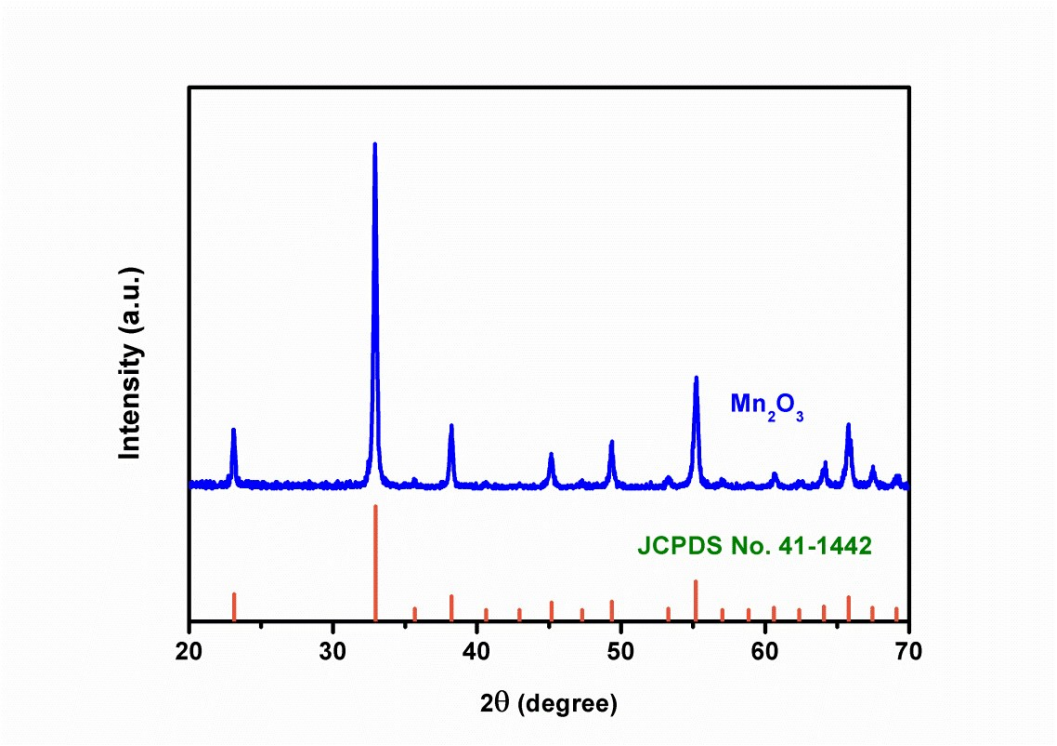

Figure S7. XRD pattern of as-prepared MnO@NDC after TGA test.

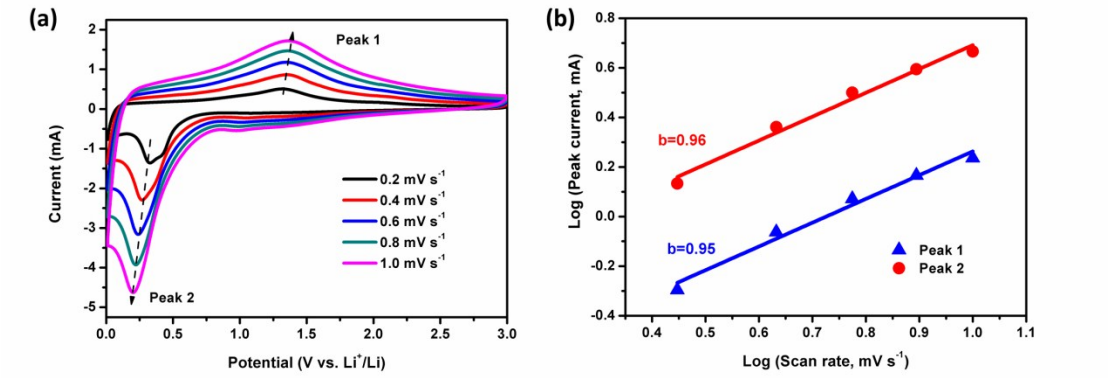

Figure S8. (a) CV curves at different sweep rates. (b) Relationship between logarithm cathodic peak current and lograrithm scan rates.

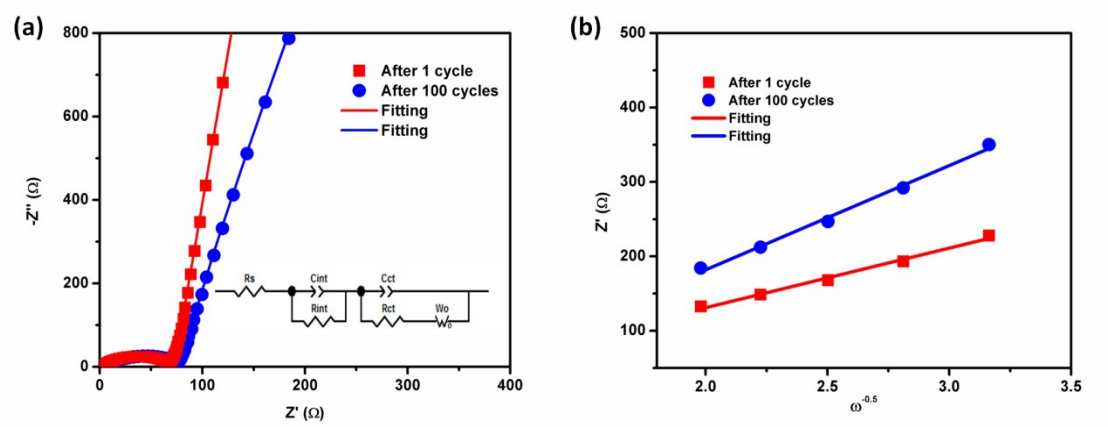

Figure S9. (a) The Nyquist plots and fitting of MnO/NDC electrode after 1 and 100 cycles for LIBs. (b) The relationship of Z' vs. $\omega^{-1/2}$ is obtained by measuring the slope of the oblique line in the low frequency region.

The Li^+ diffusion coefficient can be calculated from the formula as following:

$$D = \frac{R^2T^2}{2A^2n^4F^4C^2\sigma^2} \qquad (1)$$

R is the gas constant and F is the Faraday constant. T is the temperature of environment experiment. A is the surface area of the electrode. n is the number of the electrons per molecule. σ is the slope of the line $Z' \sim \omega^{-0.5}$. C is the lithium ion concentration in the bulk electrode:

$$C = nV = \frac{(m/M)}{V} = \frac{(\rho V/M)}{V} = \frac{\rho}{M} \qquad (2)$$

The lithium ion concentration in the bulk electrode is about 8.9×10^{-3} mol cm^{-3}.

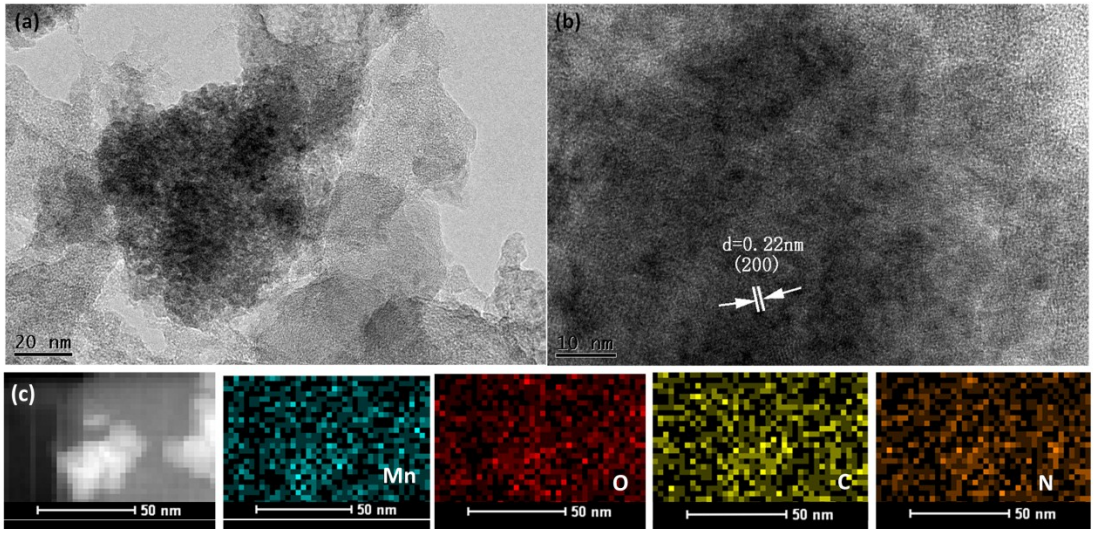

Figure S10. (a) TEM image of MnO@NDC electrode after 100 cycles. (b) HRTEM image of MnO@NDC electrode after 100 cycles. (c) EDX mapping for MnO@NDC electrode after 100 cycles.

Table S1. Comparison of the electrochemical performance for MnO-based anode in the previous literature with our sample

Electrode materials	**Rate perfomance**	**Cycling performance**	**Ref**
MnO@CNFs	407 mAh g^{-1} at 2.0 A g^{-1}	400 mAh g^{-1} at 1.0 mA g^{-1} after 500 cycles	1
MnO/C	483 mAh g^{-1} at 5.0 A g^{-1}	1625 mAh g^{-1} at 1.0 A g^{-1} after 1000 cycles	2

MnO@N-C/rGO	448.9 mAh g^{-1} at 2.0 A g^{-1}	425.0 mAh/g at 2.0 A g^{-1} after 1300 cycles	3
MnO@NCs	438.2 mAh g^{-1} at 2.0 A g^{-1}	465.8 mAh g^{-1} at 0.1 A g^{-1} after 100 cycles	4
MnO/NC	316.3 mAh g^{-1} at 2.0 A g^{-1}	568.5 mAh g^{-1} at 1.0 A g^{-1} after 500 cycles	5
MnO@C	680 mAh g^{-1} at 2.0 A g^{-1}	686.5 mAh g^{-1} at 0.2 A g^{-1} after 100 cycles	6
G/MnO@C/G	504.4 mAh g^{-1} at 4.0 A g^{-1}	471.3 mAh g^{-1} at 4.0 A g^{-1} after 4000 cycles	7
CNF/MnO	600 mAh g^{-1} at 1.0 A g^{-1}	983.8 mAh g^{-1} at 0.2 A g^{-1} after 100 cycles	8
MnO@C	252 mAh g^{-1} at 1.6 A g^{-1}	613 mAh g^{-1} at 1.0 A g^{-1} after 1000 cycles	9
MnO@C	380.1 mAh g^{-1} at 7.6 A g^{-1}	596.3 mAh g^{-1} at 3.8 A g^{-1} after 1000 cycles	10
MnO/Ni/CNF	251.2 mAh g^{-1} at 2.0 A g^{-1}	361.9 mAh g^{-1} at 1.0 A g^{-1} after 600 cycles	11
MnO@NC	454 mAh g^{-1} at 5.0 A g^{-1}	624 mAh g^{-1} at 1.0 A g^{-1} after 1000 cycles	12

MnO@NDC	**446.8 mAh g^{-1} at 10.0 A g^{-1}**	**864.8 mAh g^{-1} at 1.0 A g^{-1} after 1000 cycles**	**This work**

Table S2. EXAFS fitting parameters at the Mn K-edge for various samples（S_0^2=0.813）

Sample	Shell	N^a	R(Å)^b	σ^2(Å^2)^c	ΔE_0(eV)^d	R factor
Mn foil	Mn-Mn	12	2.66	0.0027	8.0	0.0338
	Mn-Mn	4	2.80	0.0027		
Pristine	Mn-O	5.8	2.24	0.0272	-0.5	0.0006
	Mn-Mn	6.9	3.12	0.0090		
Dischar 1.5 V	Mn-O	5.4	2.25	0.0243	0.5	0.0003
	Mn-Mn	7.6	3.11	0.0103		
Dischar 0.01 V	Mn-O	1.7	2.05	0.0228	-1.6	0.0005
	Mn-Mn	8.3	2.74	0.0475		
Char 1.5 V	Mn-O	2.2	2.06	0.0090	-6.9	0.0005
	Mn-Mn	4.6	2.82	0.0339		
Char 3.0 V	Mn-O	5.6	2.20	0.0194	-3.5	0.0008
	Mn-Mn	8.5	3.12	0.0106		

$^a N$: coordination numbers; $^b R$: bond distance; $^c \sigma^2$: Debye-Waller factors; ^{d} ΔE_0: the

inner potential correction. *R* factor: goodness of fit. S_0^2 was set to 0.813, according to the experimental EXAFS fit of MnO reference by fixing CN as the known crystallographic value.

Table S3. Equivalent circuit parameters of the MnO@NDC electrode for LIBs.

Sample	Cycle number	R_s/Ohm	R_{int}/Ohm	R_{ct}/Ohm
MnO@NDC	1st cycle	3.6	65.3	16.8
	100th cycle	8.5	69.8	15.4

References

1 L. Sheng, H. Jiang, S. Liu, M. Chen, T. Wei, Z. J. Fan, *J. Power Sources* **2018**, *397*, 325-333.

2 D. Kang, Q. Liu, R. Si, J. Gu, W. Zhang, D. Zhang, *Carbon* **2016**, *99*, 138-147.

3 W. Zhang, J. Li, J. Zhang, J. Sheng, T. He, M. Tian, Y. Zhao, C. Xie, L. Mai, S. Mu, A*CS Appl. Mater. Interfaces* **2017**, *9*, 12680-12686.

4 L. Zhang, D. Ge, G. Qu, J. Zheng, X. Cao, H. Gu, *Nanoscale* **2017**, *9*, 5451-5457.

5 Q. Ye, J. Ru, J. Peng, G. Chen, D. Wang, *Chem. Eng. J.* **2018**, *331*, 570-577.

6 J. Jia, X. Hu, Z. Wen, *Nano Res.* **2018**, *11*, 1135-1145.

7 J. Zhang, W. Zhang, T. He, I. S. Amiinu, Z. Kou, J. Li, S. Mu, *Carbon* **2017**, *115*, 95-104.

8 T. Wang, H. Li, S. Shi, T. Liu, G. Yang, Y. Chao, F. Yin, *Small* **2017**, *13*, 1604182.

9 F. Zheng, Z. Yin, H. Xia, G. Bai, Y. Zhang, *Chem. Eng. J.* **2017**, *327*, 474-480.

10 Z. Cui, Q. Liu, C. Xu, R. Zou, J. Zhang, W. Zhang, G. Guan, J. Hu, Y. Sun, *J. Mater. Chem. A* **2017**, *5*, 21699-21708.

11 X. Kong, A. Pan, Y. Wang, D. Selvakumaran, J. Lin, X. Cao, S. Liang, G. Cao, *J. Mater. Chem. A* **2018**, *6*, 12316-12322.

12 G. Zhu, L. Wang, H. Lin, L. Ma, P. Zhao, Y. Hu, T. Chen, R. Chen, Y. Wang, Z. Tie, J. Liu, Z. Jin, *Adv. Funct. Mater.* **2018**, *28*, 1800003.